Wingbeat Time and the Scaling of Passive Rotational Damping in Flapping Flight

Tyson L. Hedrick,[1]* Bo Cheng,[2] Xinyan Deng[2]*

Flying animals exhibit remarkable capabilities for both generating maneuvers and stabilizing their course and orientation after perturbation. Here we show that flapping fliers ranging in size from fruit flies to large birds benefit from substantial damping of angular velocity through a passive mechanism termed flapping counter-torque (FCT). Our FCT model predicts that isometrically scaled animals experience similar damping on a per-wingbeat time scale, resulting in similar turning dynamics in wingbeat time regardless of body size. The model also shows how animals may simultaneously specialize in both maneuverability and stability (at the cost of efficiency) and provides a framework for linking morphology, wing kinematics, maneuverability, and flight dynamics across a wide range of flying animals spanning insects, bats, and birds.

Flying animals of all sizes exhibit a surprising degree of maneuverability, and animals ranging in size from fruit flies (*1*) to pigeons (*2*) have been the subject of detailed analyses of maneuvering kinematics. Many studies have also considered stability and control in animal flight, both from a neural standpoint (*3*, *4*) and in broader analyses incorporating both neural and physical inputs (*5*–*7*). This body of work provides the opportunity to examine the scaling of maneuvering capability with body size and determine whether animals of different sizes and phylogenetic groups use similar or different mechanisms to accomplish maneuvers.

We focus our comparison on a particular type of maneuver: low-speed yaw turns of 60° or more (Fig. 1), because these have been most widely recorded in freely flying animals. Rotational maneuvers such as yaw turns necessarily include both an angular acceleration phase, where the animal begins turning, and an angular deceleration phase, where the animal slows and ends the rotation. In the acceleration phase, the animal must actively produce an aerodynamic torque through some type of flapping or body asymmetry. However, the animal might then decelerate by either actively producing a torque in the opposite direction (*1*) or simply allowing friction to passively damp out its rotational velocity, coasting to a halt. Because the moment of inertia is proportional to mass to the five-thirds power (mass$^{5/3}$), large animals such as birds are likely to require active deceleration whereas smaller animals such as flies are often modeled with substantial fluid drag (*8*), which might allow passive deceleration, although a recent report emphasizes active deceleration in these animals as well (*1*). However, other recent analyses of yaw turns in insects (*9*) and banked turns in birds (*10*) emphasized the importance of a form of aerodynamic damping related to symmetric wing motion, raising the possibility that passive damping is important at many size scales.

Damping from wing motion arises as follows: Consider an animal engaged in symmetric hovering or low-speed flight (Fig. 2, A and B). Previous experiments have shown that during downstroke, net aerodynamic forces are directed upward and posteriorly; in upstroke, in animals with an aerodynamically active upstroke, the forces are directed upward and anteriorly (*11*, *12*). However, when the animal experiences whole-body rotation (for example, about an axis normal to the plane of flapping), net wing velocity is enhanced on the outside wing during downstroke and on the inside wing during upstroke (*2*). This net velocity asymmetry, which arises when the animal is flapping symmetrically, gives rise to a force asymmetry (and therefore a torque) that acts to slow the animal's rotation (Fig. 2, C and D). We refer to this form of damping as FCT because it depends on flapping and acts counter to the direction of body rotation. Below, we explore the scaling implications of FCT by postulating a simple equation modeling FCT and a second equation modeling active torque generation via asymmetric flapping, the expected deceleration method for large animals because of the rapid increase in moment of inertia with body size. We use these two equations to develop alternative predictions of the rotational deceleration dynamics for flying animals and then compare the predictions to measurements of yaw turning in four species of insects and three species of vertebrates across six orders of magnitude in body mass (from 1×10^{-4} to 285 g). The results of the comparison are consistent with FCT but not with an active deceleration via asymmetric flapping.

The rotational damping due to FCT arises from the difference in velocity between the inside and outside wings (Fig. 2, C and D). Thus, FCT is the result of (velocity due to flapping – velocity due to body rotation)^2 on one wing minus (velocity due to flapping + velocity due to rotation)^2 on the other wing, multiplied by the determinants of aerodynamic force: air density; wing size and shape; and where flapping velocity is determined by amplitude, frequency, and trajectory. Angular deceleration resulting from FCT is therefore

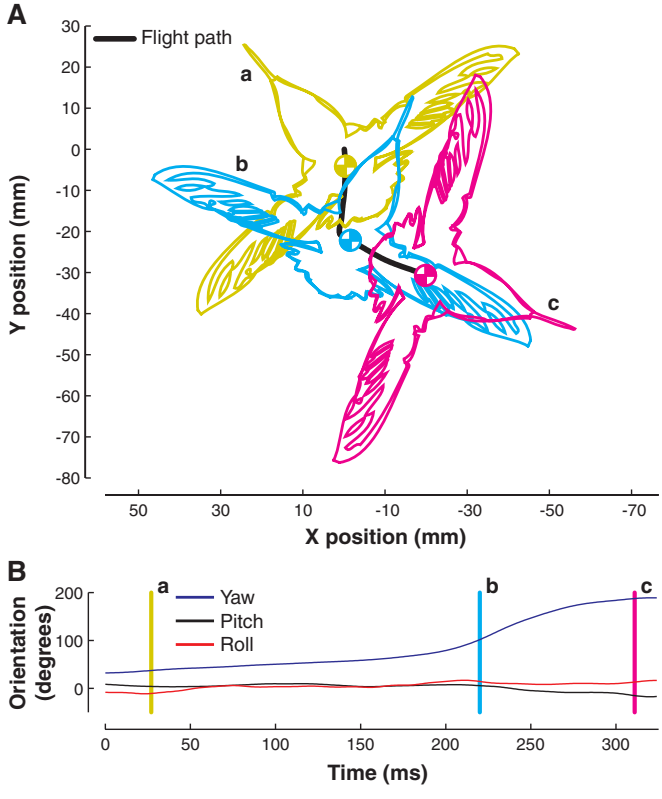

Fig. 1. A sharp yaw turn performed by a hovering ruby-throated hummingbird. (**A**) The hummingbird's position and orientation in the horizontal (*x*-*y*) plane at three different times during the turn, viewed from above the bird, looking down. The +*z* axis points into the page and toward the ground, parallel to gravity. The hummingbird yaws to its right, corresponding to a clockwise motion on the figure between stages a, b, and c. The hummingbird is to scale, but the wing position in the figure does not indicate the actual wing position. In addition to the horizontal movement depicted here, the hummingbird descended 25 mm during the recording. (**B**) The hummingbird's yaw, pitch, and roll orientation through time. The vertical lines a, b, and c indicate the time represented by each of the outline figures in (A).

[1]Department of Biology, University of North Carolina at Chapel Hill, Chapel Hill, NC 27599, USA. [2]Department of Mechanical Engineering, University of Delaware, Newark, DE 19716, USA.

*To whom correspondence should be addressed. E-mail: thedrick@bio.unc.edu (T.L.H.); deng@udel.edu (X.D.)

proportional to angular velocity and inversely proportional to the animal's moment of inertia. These factors may be expressed concisely by the following ordinary differential equation

$$\dot{\omega}_{FCT} = -\omega \frac{\rho R^4 \bar{c} \hat{r}_3^3(S) \Phi n \overline{C_F \sin(\alpha)(d\hat{\varphi}/d\hat{t})}}{I} \quad (1)$$

where $\dot{\omega}_{FCT}$ is angular deceleration due to FCT, ω is angular velocity, $\overline{C}_F$ is the mean aerodynamic resultant force coefficient, α is the spanwise rotation angle of the wing, ρ is air density, R is wing length, $\bar{c}$ is the average wing chord, $\hat{r}_3(S)$ is the nondimensional third moment of area, Φ is wing stroke amplitude, n is wingbeat frequency, $(d\hat{\phi}/d\hat{t})$ is the nondimensional wing angular velocity, and I is the animal's moment of inertia. All symbols are as per Ellington (*13*). See appendix A in (*14*) for background on this equation.

An alternative to deceleration by FCT, active torque generation by asymmetric flapping, depends on the degree of functional asymmetry between the two wings; deceleration due to asymmetric flapping may be written as

$$\dot{\omega}_a = (\gamma - 1) \frac{\rho R^4 \bar{c} \hat{r}_3^3(S) \Phi^2 n^2 \overline{C_F \sin(\alpha)(d\hat{\varphi}/d\hat{t})^2}}{8I} \quad (2)$$

where γ is the magnitude of the asymmetry, ranging from 0 to 1, with 1 indicating no asymmetry. Unlike FCT, active deceleration is not related to body angular velocity. See appendix B in (*14*) for additional details on this formulation.

It is known that the dimensions of flying animals scale at near isometry, with wing length and chord proportional to mass$^{1/3}$ and moment of inertia proportional to mass$^{5/3}$ (*15*). Wingbeat frequency is known to scale as mass$^{-0.24}$ for insects and hummingbirds, but the fit is poor and there is substantial variation within a given size range (*16*). Therefore, after assuming isometric scaling and eliminating nonvarying and nondimensional terms from Eqs. 1 and 2, we are left with the following proportionalities

$$\dot{\omega}_{FCT} \propto -\omega \Phi n \quad (3)$$

$$\dot{\omega}_a \propto (\gamma - 1) \Phi^2 n^2 \quad (4)$$

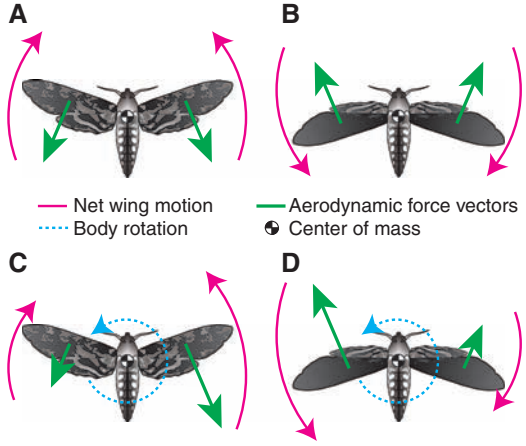

Fig. 2. FCT arises when overall body rotation interacts with symmetric wing motion. (**A**) and (**B**) show the aerodynamic forces experienced by a flying animal in upstroke (A) and downstroke (B). (**C**) and (**D**) show how wing motion and aerodynamic forces are modified by overall body rotation. The now asymmetric aerodynamic forces provide a torque counter to the body rotation.

Table 1. Morphological data and predictions from the active and passive deceleration hypotheses along with the measurements. I'_{zz}, moment of inertia of the animal in the stroke plane frame yaw axis; $t_{1/2}(N)$, half-life as a function of number of wingbeats. See (*14*) for details of the FCT and active deceleration predictions as well as the sources of the morphological and kinematic data. Active deceleration predictions are for the time required to decelerate to one-half of peak velocity, making them directly comparable to the FCT predictions. We used a γ of 0.944, based on an arithmetic solution of Eq. 2 to the fruit fly data. See (*14*) for results scaling γ to body size or other factors. For both sets of predictions, we assume that $\overline{C_F \sin(\alpha)(d\hat{\phi}/d\hat{t})}$ is equal to 6.0 and $\overline{C_F \sin(\alpha)(d\hat{\phi}/d\hat{t})^2}$ is equal to 31.3 for all species.

Species	Morphology							FCT passive deceleration predictions		Active deceleration predictions		Measurements	
	Mass (g)	I'_{zz} (N·m s^2)	R (mm)	$\bar{c}$ (mm)	n (Hz)	Φ (°)	$\hat{r}_3(S)$ (–)	$t_{1/2}(t)$ (ms)	$t_{1/2}(N)$ (wingbeats)	$t_{1/2}(t)$ (ms)	$t_{1/2}(N)$ (wingbeats)	$t_{1/2}(t)$ (ms)	$t_{1/2}(N)$ (wingbeats)
Fruit fly (*Drosophila melanogaster*)	9.6 ± 2.7 × 10^{-4}	2.72 × 10^{-13} –	2.39 ± 0.08	0.80 ± 0.02	218 ± 7	140 ± 10	0.59	9.2 ± 1.5	2.00 ± 0.32	10.4 ± 2.3	2.22 ± 0.48	10.36	2.2
Stalk-eyed fly (*Cyrtodiopsis dalmanni*)	7.0 ± 1.0 × 10^{-3}	1.60 × 10^{-11} –	4.46 ± 0.14	0.94 ± 0.08	170 ± 8	140* ± 10	0.64	38.0 ± 11.1	6.47 ± 1.85	55.1 ± 11.8	9.35 ± 1.82	35.68	5.6
Bluebottle fly (*Calliphora vicina*)	6.2 × 10^{-2} ± 5.0 × 10^{-3}	2.81 × 10^{-10} –	9.2 ± 0.5	3.14 ± 0.5	143 ± 9	138 ± 15	0.59	17.2 ± 11.7	2.43 ± 1.63	30.8 ± 15.0	4.32 ± 2.01	14.31	2.1
Hawkmoth (*Manduca sexta*)	1.62 ± 0.33	2.43 × 10^{-7} –	48.8 ± 2.1	18.6 ± 1.6	26 ± 2	98 ± 4	0.56	28.4 ± 6.6	0.74 ± 0.16	166.1 ± 46.3	4.31 ± 1.02	19	0.5†
Hummingbird (*Archilochus colubris*)	3.17 ± 0.15	3.58 × 10^{-7} –	45.0 ± 4.7	11.8 ± 2.0	48.7 ± 9.1	134 ± 7.2	0.57	33.8 ± 26.1	1.64 ± 1.13	184.1 ± 180.2	8.86 ± 6.12	45	2.0†
Fruit bat (*Cynopterus brachyotis*)	35.1 ± 1.8	4.12 × 10^{-5} –	150 ± 14	83 ± 14	11.1 ± 0.6	141 ± 14	0.54	22.0 ± 12.3	0.24 ± 0.14	415.4 ± 256.5	4.60 ± 2.77	17	0.2†
Cockatoo (*Eolophus roseicapillus*)	285.9 ± 14.4	1.29 × 10^{-3} –	347 ± 8	118 ± 4	7.1 ± 1.1	99 ± 16.4	0.58	30.3 ± 6.4	0.22 ± 0.02	945.4 ± 392.5	6.72 ± 1.37	40	0.3†

*A wingbeat amplitude measure was not available for the stalk-eyed fly; *Drosophila* kinematics were substituted. †The measurement of half-life in wingbeats uses the animal's exact wingbeat frequency when available.

where $\dot{\omega}$ is body angular deceleration due to FCT or active (a) means, ω is body angular velocity, Φ is wingbeat amplitude, n is wingbeat frequency, and γ is the magnitude of asymmetry in flapping. Wingbeat amplitude is not known to vary widely or systematically among species, whereas wingbeat frequency varies over two orders of magnitude (*15*) and from 218 to 7.1 Hz in the species examined here. Thus, variation in these equations among different species is dominated by variation in wingbeat frequency.

These equations summarize two distinct modes by which flying animals might reduce their angular velocity at the end of a maneuver. Yaw deceleration dominated by FCT would exhibit exponential decay (Eqs. 1 and 3 and eqs. S19 to S23), a pattern observed in early studies of fruit fly turning (*17*, *18*) and ascribed to body friction. For animals of approximately isometric dimensional scaling, similar wingbeat amplitudes, and similar aerodynamic force coefficients, Eq. 3 also implies that normalizing time by wingbeat frequency should result in similar wingbeat time dynamics regardless of body size (eq. S23). Deceleration due to the simple model of asymmetric flapping (Eqs. 2 and 4) is linear and occurs at a rate that varies with the square of flapping frequency.

We tested predictions of turning dynamics arising from these two modes against data from seven different animals executing low-speed yaw turns (Fig. 1 and Table 1). See appendix C in (*14*) for a description of the various sources of these data, both in the literature and from previously unreported experiments.

Unsurprisingly, given the considerable range of species examined, the different animals exhibited widely divergent yaw turning performance (Fig. 3A and Table 1), slowing down at very different rates. However, in contrast to their differences in deceleration rate, the fruit fly, stalk-eyed fly, bluebottle fly, and hummingbird all exhibited similar peak yaw rates of approximately 1600° s^{-1}. This does not appear to reflect a mechanical limitation, because Eq. 2 indicates that these animals should have greatly different capabilities for active torque generation and even different ratios of active torque to FCT (Eq. 5). It may reflect neurophysiological limitations on the rate at which flying animals can acquire and process sensory information for flight control (*19*).

The measured duration of yaw rate half-life during deceleration was similar to that predicted by the FCT passive deceleration model (Eq. 1, Table 1, and Fig. 3D). The deceleration rate, measured as the time to decelerate to one-half the peak yaw rate, was not similar to that predicted for active torque generation (Eq. 2 and Table 1). Furthermore, the prediction that approximately isometric animals should have similar rotational deceleration dynamics in wingbeat time was also supported (Fig. 2B). This prediction is specific to isometrically scaled animals; the data reveal two such groups with similar dynamics. Fruit flies, bluebottle flies, and hummingbirds have similar scaling of wing and body dimensions (table S1) and all exhibited a deceleration half-life of about two wingbeats. Hawkmoths, bats, and cockatoos all have wings approximately twice as large relative to body weight as those of the aforementioned group and all exhibited half-lives of less than a wingbeat. The stalk-eyed fly has a moment of inertia out of proportion to body size due to its unusual eye position (*20*) and had a half-life of about six wingbeats.

Our FCT model predicts yaw turn deceleration dynamics across seven phylogenetically and morphologically dissimilar flying animals spanning six orders of magnitude in body mass (Fig. 3), using only morphological and kinematic inputs, supporting FCT as a unifying principle central to the dynamics of flying animals across a large size range. Our results do not agree with a model based on deceleration via torque generation by asymmetric flapping. However, interspecific or temporal variation in asymmetry (γ) could produce the observed results—a perfectly valid although less parsimonious possibility. However, the appropriate variation in γ cannot be produced by scaling it from any of the measured morphological parameters [appendix D in (*14*) and fig. S3].

In addition to providing a framework for assessing animal flight dynamics, FCT also provides insights into form/function relationships. For example, maneuverability and stability are often cast in opposition to one another, but some factors that enhance maneuverability would also enhance FCT, a form of passive stability. The scaling of rotational maneuverability may be approximated by the same equation we use to estimate the scaling of deceleration via active torque generation (Eq. 2). Thus, increases in wingbeat frequency (n) in particular improve both an animal's aerodynamic capacity for torque generation

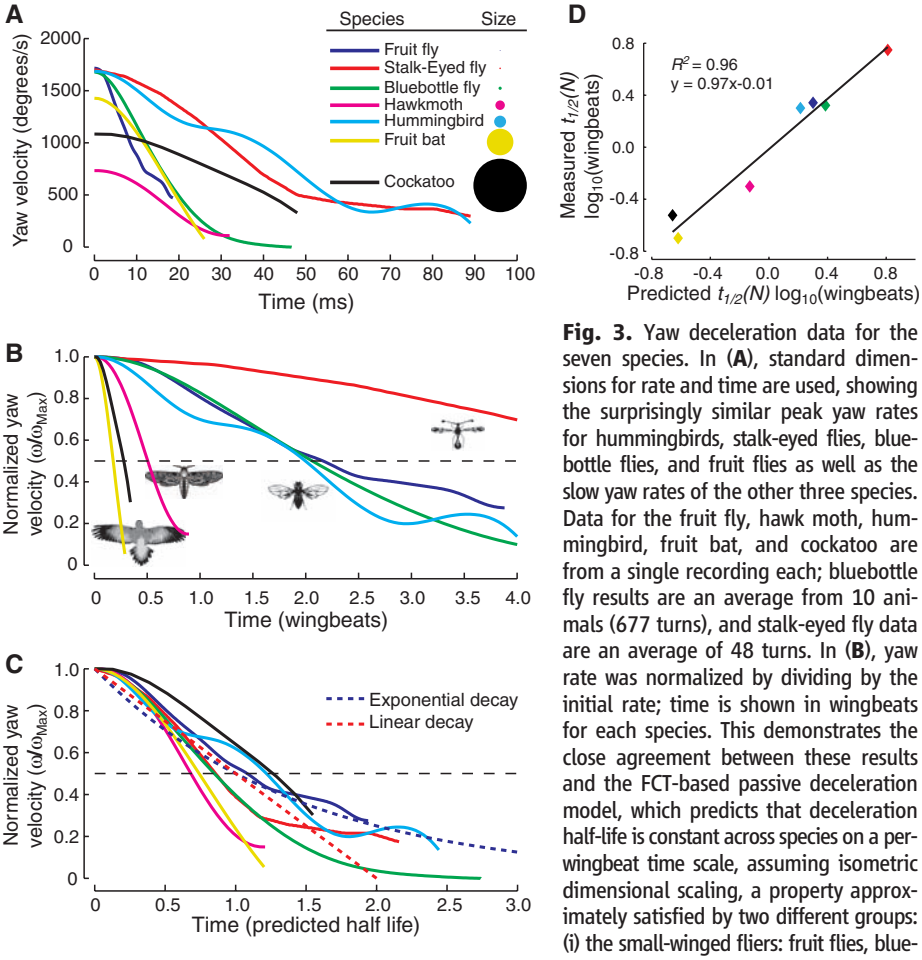

Fig. 3. Yaw deceleration data for the seven species. In (**A**), standard dimensions for rate and time are used, showing the surprisingly similar peak yaw rates for hummingbirds, stalk-eyed flies, bluebottle flies, and fruit flies as well as the slow yaw rates of the other three species. Data for the fruit fly, hawk moth, hummingbird, fruit bat, and cockatoo are from a single recording each; bluebottle fly results are an average from 10 animals (677 turns), and stalk-eyed fly data are an average of 48 turns. In (**B**), yaw rate was normalized by dividing by the initial rate; time is shown in wingbeats for each species. This demonstrates the close agreement between these results and the FCT-based passive deceleration model, which predicts that deceleration half-life is constant across species on a per-wingbeat time scale, assuming isometric dimensional scaling, a property approximately satisfied by two different groups: (i) the small-winged fliers: fruit flies, bluebottle flies, and hummingbirds; and (ii) the large-winged fliers: hawk moths, bats, and cockatoos. See table S1 for a comparison of wing and body scaling among these species. In (**C**), yaw rate is normalized as in (B) and time is normalized to the predicted half-life of each species (Table 1). Ideal exponential decay (FCT) and linear decay (asymmetric flapping) curves are also shown. (**D**) compares the predicted and measured yaw deceleration half-life across the seven species. $t_{1/2}(N)$, half-life as a function of number of wingbeats. As expected, there was a strong relationship between predicted and measured values, and the least-squares regression slope is similar to 1.0 and the regression intercept close to 0, showing that the FCT model accurately predicts deceleration half-life for this group of species, despite the wide range of body sizes, differences in body and wing morphology, and phylogenetic distance.

and the magnitude of FCT. Because active torque is proportional to n^2 and passive torque to n, the ratio of active to passive torque increases as n increases (Eq. 5), even while both quantities increase individually

$$\frac{\dot{\omega}_a}{\dot{\omega}_{FCT}} = -(\gamma - 1)\frac{\Phi n \overline{(d\hat{\varphi}/d\hat{t})}}{8\omega} \quad (5)$$

The increase in the ratio indicates an enhanced capability for active maneuvers and active stabilization, whereas the increase in FCT adds to passive stability. Thus, increasing wingbeat frequency enhances both maneuverability and stability. Hummingbirds provide an interesting example; males typically have greater wingbeat frequencies (*21*) and smaller body sizes as compared to females of the same species, potentially conferring a benefit in maneuverability and therefore an advantage in display flights (*22*) as well as greater stability when experiencing an external perturbation. These benefits are not without cost, because increasing wingbeat frequency increases the inertial and profile power requirements of flapping flight.

Finally, the success of our FCT model in predicting yaw deceleration dynamics implies that passive damping may be important to flight control in flying animals across a wide range of body sizes. For example, if a steadily flapping animal experiences a brief perturbation in midstroke, by the time it is prepared to execute a corrective wingbeat, FCT will have eroded much of the effect of the perturbation, regardless of the wingbeat frequency employed by the animal. Thus, FCT provides open loop stability for some aspects of animal flight, reducing its neuromuscular and neurosensory requirements. These are not eliminated, because FCT results in asymmetric forces from symmetric flapping, implying that the animal's muscles must generate asymmetric forces and suggesting neural regulation to enforce symmetry. Furthermore, FCT does not address all the stability problems faced by flying animals. This study is limited to yaw dynamics in hovering or slow-speed flight; FCT is likely to be influential in fast forward flight, but no data are available to test such predictions. More important, a full description of body dynamics involves many factors beyond FCT and includes modes such as pitching and longitudinal dynamics known to be inherently unstable in open loop conditions (*23*, *24*) and subject to active control (*25*, *26*). Finally, yaw damping due to FCT is a feature of flapping flight that is not found in human-made fixed-wing or rotary-wing flyers and may lead to improvements in the stability and maneuverability of biomimetic micro–air vehicles.

References and Notes

1. S. N. Fry, R. Sayaman, M. H. Dickinson, *Science* **300**, 495 (2003).
2. D. R. Warrick, K. P. Dial, *J. Exp. Biol.* **201**, 655 (1998).
3. M. F. Land, T. S. Collett, *J. Comp. Physiol. A* **89**, 331 (1974).
4. J. W. S. Pringle, in *Insect Flight*, M. Abercrombie, P. B. Medawar, G. Salt, M. M. Swann, V. B. Wigglesworth, Eds. (Cambridge Monographs in Experimental Biology, Cambridge Univ. Press, London, 1957), pp. 86–118.
5. G. K. Taylor *et al.*, *J. Exp. Biol.* **211**, 258 (2008).
6. G. K. Taylor, *Biol. Rev. Camb. Philos. Soc.* **76**, 449 (2001).
7. H. Wagner, *Philos. Trans. R. Soc. London Ser. B* **312**, 527 (1986).
8. N. Boeddeker, M. Egelhaaf, *J. Exp. Biol.* **208**, 1563 (2005).
9. T. Hesselberg, F.-O. Lehmann, *J. Exp. Biol.* **210**, 4319 (2007).
10. T. L. Hedrick, A. A. Biewener, *J. Exp. Biol.* **210**, 1897 (2007).
11. S. P. Sane, *J. Exp. Biol.* **206**, 4191 (2003).
12. J. R. Usherwood, C. P. Ellington, *J. Exp. Biol.* **205**, 1565 (2002).
13. C. P. Ellington, *Philos. Trans. R. Soc. London Ser. B* **305**, 41 (1984).
14. See supporting material on *Science* Online.
15. C. H. Greenewalt, *Smithson. Misc. Collect.* **144**, 1 (1962).
16. R. Dudley, *The Biomechanics of Insect Flight. Form, Function, Evolution* (Princeton Univ. Press, Princeton, NJ, 2000).
17. M. Mayer, K. Vogtmann, B. Bausenwein, R. Wolf, M. Heisenberg, *J. Comp. Physiol. A* **163**, 389 (1988).
18. H. H. Bülthoff, T. Poggio, C. Wehrhahn, *Z. Naturforsch. C* **35**, 811 (1980).
19. G. K. Taylor, H. G. Krapp, in *Insect Mechanics and Control*, J. Casas, S. J. Simpson, Eds. (Academic Press, London, 2007), vol. 34, pp. 231–316.
20. G. Ribak, J. Swallow, *J. Comp. Physiol. A* **193**, 1065 (2007).
21. T. A. Hunter, J. Picman, *Condor* **107**, 570 (2005).
22. F. G. Stiles, D. L. Altshuler, R. Dudley, *Auk* **122**, 872 (2005).
23. G. K. Taylor, A. L. R. Thomas, *J. Theor. Biol.* **214**, 351 (2002).
24. M. Sun, J. K. Wang, *J. Exp. Biol.* **210**, 2714 (2007).
25. G. K. Taylor, A. L. R. Thomas, *J. Exp. Biol.* **206**, 2803 (2003).
26. X. Deng, L. Schenato, S. S. Sastry, *IEEE Trans. Robotics* **22**, 789 (2006).

27. We thank A. Biewener of Harvard University and S. Swartz and K. Breuer of Brown University for providing the hummingbird and fruit bat data. This work was funded in part by NSF grant 0732267 (Division of Integrative Organismal Systems) to T.L.H. and NSF grant 0545931 (Division of Information and Intelligent Systems) to X.D.

Supporting Online Material

www.sciencemag.org/cgi/content/full/324/5924/252/DC1
SOM Text
Figs. S1 to S3
Table S1
References
Appendices A to D

12 November 2008; accepted 20 February 2009
10.1126/science.1168431

Coding-Sequence Determinants of Gene Expression in *Escherichia coli*

Grzegorz Kudla,[1]* Andrew W. Murray,[2] David Tollervey,[3] Joshua B. Plotkin[1]†

Synonymous mutations do not alter the encoded protein, but they can influence gene expression. To investigate how, we engineered a synthetic library of 154 genes that varied randomly at synonymous sites, but all encoded the same green fluorescent protein (GFP). When expressed in *Escherichia coli*, GFP protein levels varied 250-fold across the library. GFP messenger RNA (mRNA) levels, mRNA degradation patterns, and bacterial growth rates also varied, but codon bias did not correlate with gene expression. Rather, the stability of mRNA folding near the ribosomal binding site explained more than half the variation in protein levels. In our analysis, mRNA folding and associated rates of translation initiation play a predominant role in shaping expression levels of individual genes, whereas codon bias influences global translation efficiency and cellular fitness.

The theory of codon bias posits that preferred codons correlate with the abundances of iso-accepting tRNAs (*1*, *2*) and thereby increase translational efficiency (*3*) and accuracy (*4*). Recent experiments have revealed other effects of silent mutations (*5*–*7*). We synthesized a library of green fluorescent protein (GFP) genes that varied randomly in their codon usage, but encoded the same amino acid sequence (*8*). By placing these constructs in identical regulatory contexts and measuring their expression, we isolated the effects of synonymous variation on gene expression.

The GFP gene consists of 240 codons. For 226 of these codons, we introduced random silent mutations in the third base position, while keeping the first and second positions constant (Fig. 1A). The resulting synthetic GFP constructs differed by up to 180 silent substitutions, with an average of 114 substitutions between pairs of constructs (Fig. 1B and figs. S1 and S2). The range of third-position GC content (GC3) across the library of constructs encompassed virtually all (99%) of the GC3 values among endogenous *Escherichia coli* genes, and the variation in the codon adaptation index (CAI) (*9*) contained most (96%) of the CAI values of *E. coli* genes (Fig. 1).

We expressed the GFP genes in *E. coli* using a T7-promoter vector, and we quantified expression by spectrofluorometry. Fluorescence levels varied 250-fold across the library, and they were highly reproducible for each GFP construct (Spearman $r = 0.98$ between biological replicates) (fig. S3). Fluorescence variation was consistent across a broad range of experimental conditions (fig. S4).

[1]Department of Biology and Program in Applied Mathematics and Computational Science, The University of Pennsylvania, Philadelphia, PA 19104, USA. [2]Department of Molecular and Cellular Biology, Harvard University, Cambridge, MA 02138, USA. [3]Wellcome Trust Centre for Cell Biology and Centre for Systems Biology, University of Edinburgh, Edinburgh EH9 3JR, UK.

*Present address: Wellcome Trust Centre for Cell Biology, University of Edinburgh, Edinburgh EH9 3JR, UK.
†To whom correspondence should be addressed. E-mail: jplotkin@sas.upenn.edu